Available online at www.sciencedirect.com
ScienceDirect
Trans. Nonferrous Met. Soc. China 27(2017) 779−788
Transactions of Nonferrous Metals Society of China
www.tnmsc.cn

Fabrication of Al/Al_2Cu in situ nanocomposite via friction stir processing

M. AZIZIEH[1], D. IRANPARAST[1], M. A. G. DEZFULI[1], Z. BALAK[1], H. S. KIM[2]

1. Department of Materials Science and Engineering, College of Engineering, Ahvaz Branch, Islamic Azad University, Ahvaz 61349-37333, Iran;
2. Department of Materials Science and Engineering, Pohang University of Science and Technology (POSTECH), Pohang 790−784, Korea

Received 17 March 2016; accepted 28 May 2016

Abstract: The aim of present work is fabrication of Al/Al_2Cu in situ nanocomposite by friction stir processing (FSP) as well as investigation of FPS parameters such as rotational speed, travel speed, number of FSP passes, and pin profile on the microstructure, chemical reaction, and microhardness of Al based nanocomposite. The Al_2Cu particles were formed rapidly due to mechanically activated effect of FSP as well as high heat generation due to Al−Cu exothermic reaction. The microstructure of the nanocomposites consisted of a finer grained aluminium matrix (~15 μm), unreacted Cu nanoparticles (~40 nm), and reinforcement nanoparticles of Al_2Cu. Irregular morphology of Al_2Cu is attributed to the local melting during FSP. Pin diameter has a higher effect on the microstructure and hardness values. The hardness measurements exhibited enhancement by 57% compared with the base metal.
Key words: friction stir processing; composite materials; hardness; microstructure; surface properties

1 Introduction

Metal matrix composites (MMCs) are of great interest for structural and electrical applications considering their industrially feasible processing, low cost, and superior properties [1,2]. Applications of MMCs are dealing with utilizing nanometric reinforcements and refining the grain structure in order to activate higher strength with reasonable ductility [3]. Numerous studies have been performed on the microstructure−property relationship in various metal−matrix nanocomposites [4,5].

Recently, aluminium matrix nanocomposites have intensively been studied [6]. These nanocomposites are fabricated via various techniques that can be classified into solid state, liquid state, and deposition processes [7]. An almost new approach is friction stir processing (FSP), which has recently attracted a great attention for the fabrication of MMCs on surfaces of base metals [8]. Many feasibility studies have been performed on the processing of aluminium matrix nanocomposites [9,10] as well as many other systems [11]. In this process, a non-consumable tool with a concentric shoulder and specific pin design is plunged into the metal matrix workpiece [12]. By adding the second phase nanoparticles ahead of the tool during processing, surface modifications are attained [13]. Due to severe plastic deformation which promotes mixing and refining of the constituent phases in the material, and elevated temperature that facilitates the chemical reactions [14], the FSP can be used as an in situ composite fabrication process.

Recently, Al−Al_2Cu [15,16], Al−Al_3Ni [17,18], Al−Al_3Fe [19], and Al−Al_3Ti [20−22] in situ composites have been successfully fabricated by employing FSP on Al−Cu, Al−Ni, Al−Fe, and Al−Ti elemental powder mixtures, respectively. In these reports, the role of the in situ formed particles on the microstructural evolutions and mechanical properties has been reported in details. However, the effects of FSP parameters such as rotational speed, travel speed, number of FSP passes, and pin profile on the intermetallics formation were not studied.

The aim of this work is to study the chemical reaction and dissolution of copper nanoparticles in the Al matrix during severe plastic deformation and heat flow upon FSP. The effects of rotational speed, number of FSP passes, and pin diameter on the in situ chemical reactions and its role on the formation of intermetallic phases are

Corresponding author: M. AZIZIEH; Tel: +98-912-3798088; E-mail: azizieh@iauahvaza.ac.ir
DOI: 10.1016/S1003-6326(17)60089-X

elaborated. Additionally, the microhardnesses of the nanocomposites are examined and compared with those of the base metal.

2 Experimental

Commercial aluminium alloy (rolled 1100 Al) with the thickness of 10 mm was used in the current study. The material was cut into sheet of 110 mm × 70 mm. Copper powders with a commercial purity of 99.9%, and an average particle diameter of 40 nm were used as nanoparticle additives. On the surface of the Al plate, a groove with a width of 0.7 mm and depth of 5 mm was machined and filled with the copper powders of ~0.4 g. After tapping with hand, a capping FSP pass was performed by employing a tool with a shoulder (18 mm in diameter) having no pin. The FSP tool was made of H13 steel with a concave shape shoulder (diameter of 18 mm and concave angle of 8°) and a cylindrical threaded pin (height of 6 mm, diameters of 4, 5, and 6 mm). Rotational speeds of 1120 and 1800 r/min and a travel speeds of 56 and 112 mm/min were used. The tool angle with respect to the normal axis of the sample plane was kept around 2°. Multi-pass FSPs (2, 4, and 6 passes) were performed in order to uniformly incorporate the Cu particles into the Al matrix and to pursue Al/Cu solid state chemical reactions. The processing conditions were not changed for the repeated passes but 100% overlap was considered. The pressing depth of the tool shoulder for each FSP pass was set to be ~0.2 mm. A K-type thermocouple was placed at the bottom of the samples at the centreline for temperature recording during the welding process.

For microstructural examinations, the processed samples were cross-sectioned perpendicular to the FSP direction. Standard metallographic procedures were employed through grinding with SiC papers followed by polishing with diamond paste. The polished cross-sections were chemically etched using Keller reagent. Microstructural studies were examined using stereographic and optical microscopes. The average grain size of different regions was measured using the mean linear intercept method. Further microstructural examinations were performed using field emission-scanning electron microscopy (FE-SEM) and intermetallic phases were investigated by energy dispersive X-ray spectroscopy (EDS) analysis and X-ray diffractometer (XRD).

The hardness profile along the FSP-processed samples was recorded on the metallographic cross-sections utilizing a Vickers micro-hardness indenter. The measurement was performed underneath the top surfaced with 2 mm distance. The applied load was 200 g with 15 s dwell time.

3 Results and discussion

3.1 Macrostructure

The typical surface appearance of the FSPed aluminium base nanocomposite is presented in Fig. 1. As can be seen, a smooth appearance without depressions was successfully produced. Semicircular features, close to those formed during the conventional FSW process are seen. As KRISHNAN [23] described, the space between the semi-circular was approximately travel-to-rotation speed ratio.

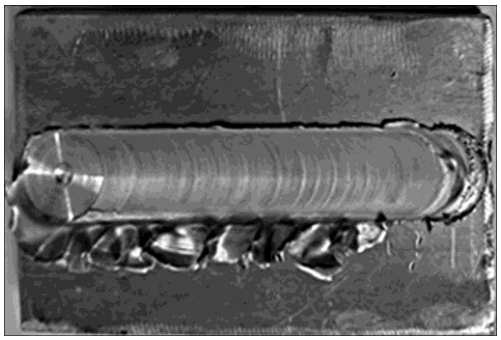

Fig. 1 Typical surface appearance of FSPed aluminium base nanocomposite

The variation of macrostructure of the surface composite cross-section in various processing conditions is presented in Fig. 1. It is evident that the pin diameter and the number of FSP passes influenced the area of surface composite to a certain extent. With increasing the pin diameter, the area of the surface composite increased. This area was measured using an image analysing software. As shown in Table 1, due to an increase in the surface composite area, the volume fractions of copper particles added to the substrate were 7.0%, 5.4%, and 4.4% in the samples FSPed using the tools with 4, 5, and 6 mm pin diameters, respectively. The increase of the area of the surface composite can be explained as follows: With the increase in the pin diameter as a result of higher pin surface, the heat input was increased due to increase of frictional heat generation and higher materials plastic deformation. As a consequence, higher materials flow results in higher stir zone volume. Also as illustrated in Fig. 3, a reduction in pin diameter leads to heterogeneous distribution and aggregation of nanoparticles in the bottom of the stir zone. This is due to a reduction of linear speed of the pin thread with a decrease in the pin diameter and therefore low downward force which reduces the circulation of the materials.

Figure 2 also reveals the effect of rotational and travel speed as well as number of FSP passes on the stir zone configuration and nanoparticles distribution. With the increase of rotational-to-travel speed ratio, the heat input and plastic deformation increase and therefore

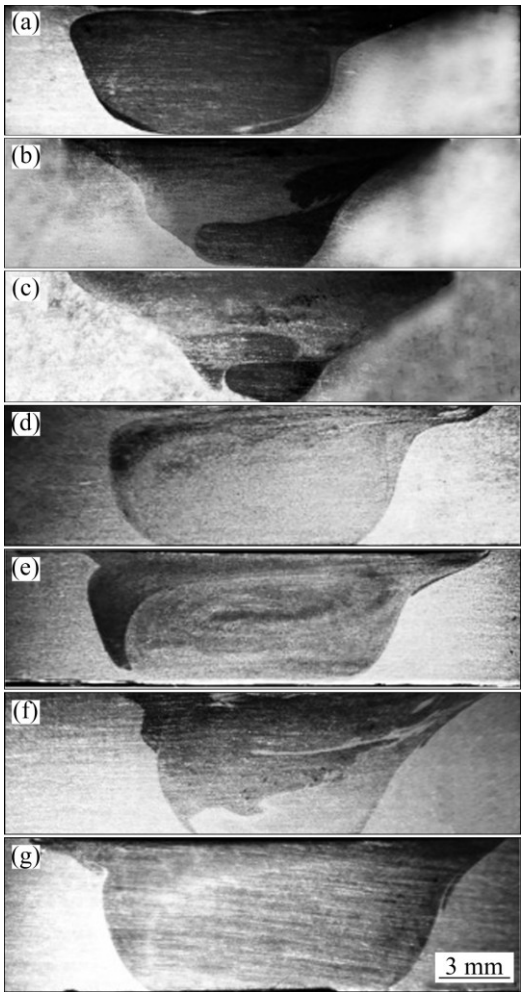

Fig. 2 Effect of rotational speed, travel speed, number of FSP passes, and pin profile on macrostructure of joints: (a) 1120 r/min, 56 mm/min, 2-pass, 6 mm; (b) 1120 r/min, 56 mm/min, 2-pass, 5 mm; (c) 1120 r/min, 56 mm/min, 2-pass, 4 mm; (d) 1800 r/min, 56 mm/min, 4-pass, 5 mm; (e) 1120 r/min, 56 mm/min, 4-pass, 5 mm; (f) 1120 r/min, 112 mm/min, 4-pass, 5 mm; (g) 1120 r/min, 56 mm/min, 6-pass, 5 mm

higher material flow leads to more homogeneous distribution of nanoparticles. Also, further FSP passes have the same effects. In this case, more FSP passes, i.e., more material flow and severer deformation in the stir zone, may shatter Cu particles during the process. It is worthy to note that even after the 2nd pass of FSP using the tool with 6 mm pin diameter, the homogeneity is higher than that in the samples FSPed using the tool with 5 mm pin diameter after the 4th pass at 1800 r/min or even after the 6th pass at 1120 r/min. This result shows that the tool design is more effective than the rotational speed or number of FSP passes as mentioned in the previous reports [24].

It is further evident in Fig. 2 that the macrostructure of the surface composites does not have any notable defects such as tunnels or pin holes. The sufficient stirring action of the rotating tool causes an interaction between the plasticized aluminium substrate and copper nanoparticles which results in the formation of the surface composite. The amount of plastic deformed material and the subsequent material flow behaviour play a crucial role to obtain defect free surface composites.

3.2 Microstructure

The effect of FSP parameters on the microstructure of surface composites is shown in Fig. 3. The optical micrographs of the FSPed samples display dynamically recrystallized microstructure and also almost uniform distribution of reinforcement particles. The uniform distribution of the reinforcement particles can be attributed to adequate generation of frictional heat, stirring, and plastic flow across the stir zone.

By comparing the as-received and FSPed samples, it is evident that the FSP significantly refined the grains of the aluminium substrate. The microstructure of the rolled Al base metal consists of the columnar grains (Fig. 3). However, in the FSPed samples, an equiaxed grain structure can be observed. The average grain size of the FSPed samples is summarized in Table 1, measured using the linear intercept method. The grain refinement can be attributed to the pinning effect of reinforcement particles which impede the grain growth by suppressing grain boundary sliding [25]. Furthermore, continuous dynamic recrystallization during FSP, due to high stacking fault energy of aluminium, results in smaller grain size. Therefore, the factors influencing the dynamic recrystallization would determine the resultant microstructure of the FSP samples.

For Al alloys, increasing the tool rotation speed or the tool rotational-to-traverse speed ratio, which introduces higher heat input during FSP, would result in the coarser grains [24]. However, for the nanoparticle reinforced MMCs, the grain microstructures of the FSP samples are influenced not only by the heat input during FSP but also by the reinforcing nanoparticles. The nanoparticles would pin the grain boundaries and then inhibit the growth of the recrystallized grains [11]. As can be seen in Table 1, the increase in the tool rotational-to-traverse speed ratio, which resulted in the combined effect on the heat input and the pining effect of nanoparticles, did not exert obvious influence on the matrix grain size of the in situ composites. In the samples of FSP at 1120 r/min and 56 mm/min, the finest grain structure was made comparing with the higher or lower tool rotational-to-travel speed ratio case. Similar results were reported by YOU et al [22] in the in situ nano-Al_2O_3 reinforced Al composites fabricated from Al−SiO_2 system by FSP.

Figure 3 shows that increasing the tool rotation rate

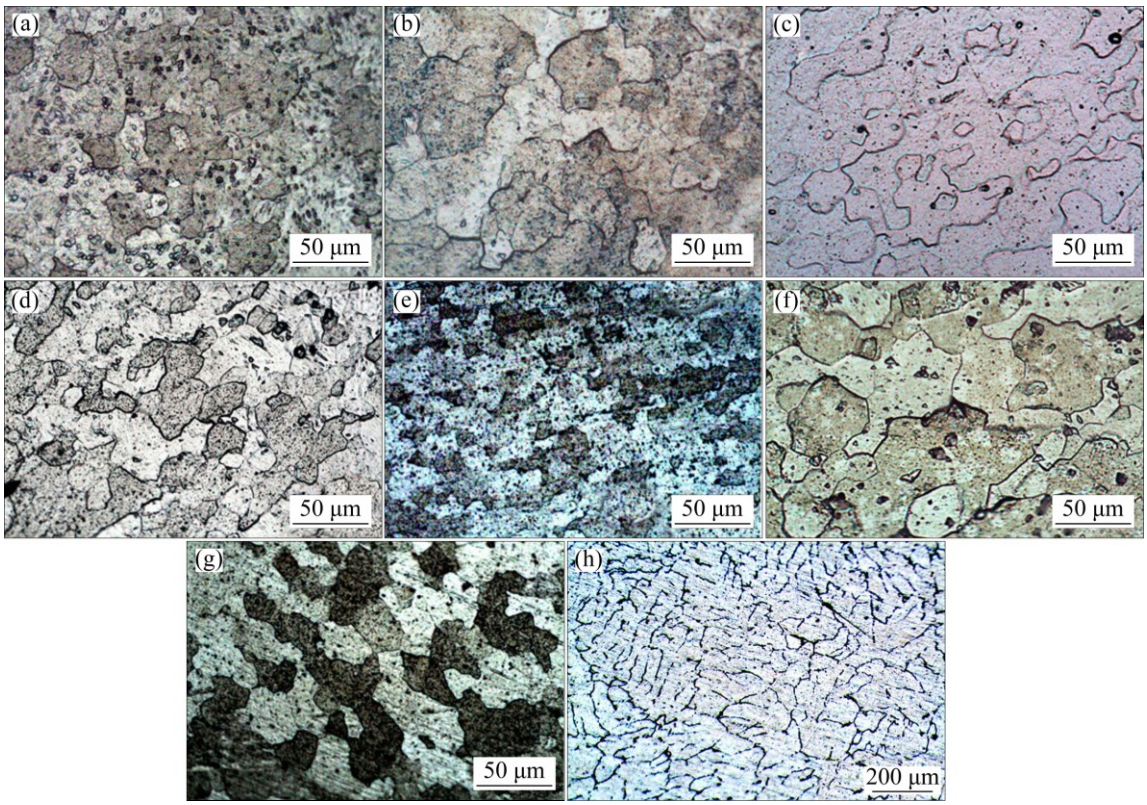

Fig. 3 Effect of rotational speed, travel speed, number of FSP passes, and pin profile on microstructure of joints: (a) 1120 r/min, 56 mm/min, 2-pass, 6 mm; (b) 1120 r/min, 56 mm/min, 2-pass, 5 mm; (c) 1120 r/min, 56 mm/min, 2-pass, 4 mm; (d) 1800 r/min, 56 mm/min, 4-pass, 5 mm; (e) 1120 r/min, 56 mm/min, 4-pass, 5 mm; (f) 1120 r/min, 112 mm/min, 4-pass, 5 mm; (g) 1120 r/min, 56 mm/min, 6-pass, 5 mm; (h) As-received

Table 1 Hardness and grain size values of FSPed samples for different processing conditions

Rotational speed/ ($r \cdot min^{-1}$)	Travel speed ($mm \cdot min^{-1}$)	FSP pass	Pin diameter/ mm	Cu volume fraction/ %	Average grain size/μm	Average hardness (HV)	Hall−Petch hardness (HV)	Difference of average and Hall−Petch hardness (HV)	Peak temperature/ K	ε^{o}/s^{-1}	$\ln Z$
1120	56	2	5	5.6	19.2	37.8	22.33	15.46	741	29.32	23.31
1120	56	4	5	5.4	9.9	43.7	24.03	19.66	741	29.32	23.31
1120	56	6	5	5.1	18.0	48.9	22.47	26.42	741	29.32	23.31
1800	56	4	5	5.0	13.4	41.1	23.19	17.90	782	47.12	22.76
1120	112	4	5	5.8	25.9	38.6	21.73	16.86	714	29.32	24.07
1120	56	2	4	7.0	15.7	35.4	22.79	12.60	733	24.43	23.37
1120	56	2	6	4.4	16.24	45.7	22.71	22.98	753	34.20	23.17

from 1120 to 1800 r/min, which increased the heat input during FSP, still caused little influence on the grain size of the matrix. This may be attributed to two factors. Firstly, a previous study [27] indicated that, although increasing the tool rotation rate would increase the peak temperature of the stir zone during FSP, the temperature rise would become slow at the high rotation rate. In the present study, the peak temperature increased from 741 to 782 K with an increase of rotational speed from 1120 to 1800 r/min. TANG et al [27] indicated that the peak temperature in the stir zone increased by almost 40 K with increasing tool rotational speed from 300 to 650 r/min, whereas it increased only 20 K when the tool rotational speed increased from 650 to 1000 r/min. Secondly, with an increase of rotational-to-travel speed ratio due to the higher material flow, the nanoparticles distribution was improved which results in a decrease of grain growth. That is, increasing the tool rotation speed almost did not coarsen the matrix grains. On the other hand, a great grain coarsening was observed in the

samples FSPed at 1120 r/min and 112 mm/min. In this case, decrease of rotational-to-travel speed ratio decreased the peak temperature to 714 K. Therefore, grain growth could occur. Also, due to low material flow, the nanoparticles could not be completely distributed and, therefore, the grain boundary migration could not be properly impeded by these particles.

As Table 1 shows, the increase of FSP passes has no linear effect on the grain size of the matrix. The average grain sizes of the samples FSPed at 1120 r/min and 56 mm/min after 2, 4, and 6 passes were 19.2, 9.9, and 18.0 μm, respectively. With an increase of FSP passes from 2 to 4, the grain size decreases due to the improvement of nanoparticle distributions. The nanoparticles can provide suitable sites to enhance the nucleation rate of new grains at the beginning of discontinuous dynamic recrystallization by particulate stimulated nucleation (PSN), and subsequently the rate of grain boundary migration would have been hindered by Zener−Holloman pinning (ZHP) [26]. Both of these PSN and ZHP mechanisms lead to enhanced grain refinement during FSP.

However, after 6 passes of FSP, a coarser grain structure occurred. According to the previous studies [28], the particles with diameter lower than 100 nm cannot act as nucleation sites. Therefore, these particles could control the grain size of the matrix by the pinning effect only. Increase of FSP passes from 4 to 6 could increase the fraction of particles with diameter lower than 100 nm and consequently the recrystallization nucleation was decreased.

As can be seen in Table 1, the average grain sizes of the samples after 2 passes of FSP by tools with pin diameters of 4, 5, and 6 mm were 15.7, 19.2, and 16.24 μm, respectively. According to the table, with an increase of pin diameter, the Zenner−Holman parameter (Z) decreased. The Z parameter has an inverse relation with the grain size [27]. Hence, with an increase of pin diameter from 4 to 5 mm, the Z parameter was decreased. Therefore, grain growth occurred. However, in the sample FSPed with 6 mm pin diameter in spite of reduction of the Z parameter, improvement of reinforcement distribution reduced the grain growth.

The microstructures of the FSPed specimens were observed using SEM/BEI, as shown in Fig. 4. The white regions are pure Cu which has been verified using energy dispersive spectroscopy (EDS), and the grey regions are Al_2Cu particles which are uniformly dispersed in the Al matrix. The microstructure observations indicate that Cu nearly completely reacted with Al to form fine Al_2Cu particles during a short FSP time. In the present study, the range of peak temperatures was 733−782 K. Because copper powders have a lower thermal conductivity than that of a solid one and considerable heat is released due to the formation of Al_2Cu particles, the local peak temperature during the FSP may be higher than the measured ones. In addition to high temperature, the material flow patterns in FSP were observed to be complex spirals and vortex-like. Therefore, it is suggested that FSP can provide: 1) severe plastic deformation, which not only promotes mixing and refining of constituent phases in the sample, but also increases the diffusion rate of elements, thereby accelerating the reaction between Al and Cu, and 2) elevated temperature, which accelerated the reaction of Al and Cu to form Al_2Cu particles.

Based on the irregular morphology of the interface between Cu and the reaction zone shown in Fig. 4(b), one may suspect that liquid phase might have been present at the Al/Cu interface. In the present study, according to CHANG et al [29], the strain rate of the FSP is 24−47 s^{-1}, which can shear the metal powders and break the oxide film surrounding Cu particles and therefore causes intimate contact between Al and Cu.

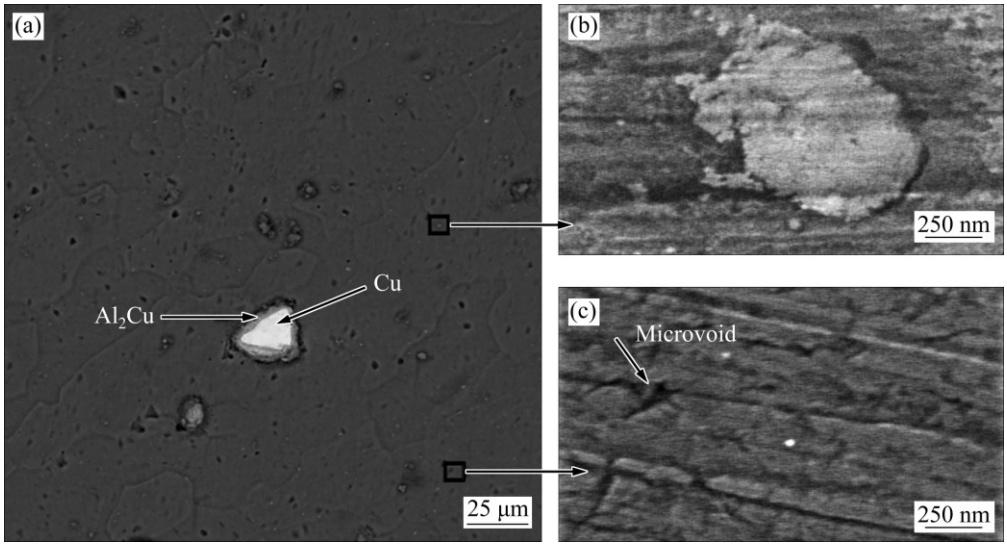

Fig. 4 SEM images of FSPed specimen

Moreover, the heat provided by the friction stirring of the rotating tool can raise the temperature high enough to initiate the exothermic reaction between Al and Cu. The heat release due to the exothermic reaction can raise the temperature and accelerate the reaction. The heat release may be high enough to cause local melting of Al at the Al/Cu interface, which can enhance the reaction. Moreover, the rotating tool in FSP could remove the reaction products from the interface and disperse them into the matrix. These are the critical mechanisms responsible for the rapid reaction and the formation of Al_2Cu in the composites produced by FSP. The current work has demonstrated that the combination of FSP and chemical reaction could be a potential technique to produce Al-matrix composites.

It may be interesting to mention that even after the 6th pass of FSP, some microvoids are formed in the stir zone as illustrated in Fig. 4. In the report of SARKARI KHORRAMI et al [19] studying the effect of SiC nanoparticles on the microstructure evolutions in the stir zone of aluminium, some voids were formed after the 1 and 2 passes of FSP.

3.3 Microhardness

The effect of FSP parameters on the microhardness of the surface composites is shown in Fig. 5. The microhardness was found to be HV 35−50 in different FSP conditions. The presence of Al_2Cu particles enhances the hardness. These reinforcement particles increase the dislocation density in aluminium matrix [30]. The interaction between these particles and dislocations increases the microhardness of the composite. As can be seen in Fig. 5(a), with an increase of the pin diameter, increased microhardness was obtained. When the pin diameter increases, the number of dislocations increases due to the higher plastic deformation. This leads to higher interactions between reinforcement particles and dislocations, which results in further increase of microhardness. Moreover, with the increase of pin diameter owing to increased materials flow and heat input, more Al_2Cu is produced and reinforcement distribution becomes homogeneous. In all, these factors increase the hardness values.

Figure 5(b) shows the effect of the number of FSP passes on the microhardness. As can be seen, further FSP results in higher microhardness values as well as wider stir zone area. Similar to the increase of pin diameter, more FSP passes caused more Al_2Cu formation and improved particles distribution. Figures 5(c) and (d) illustrate the effect of rotation-to-travel speed ratio on the

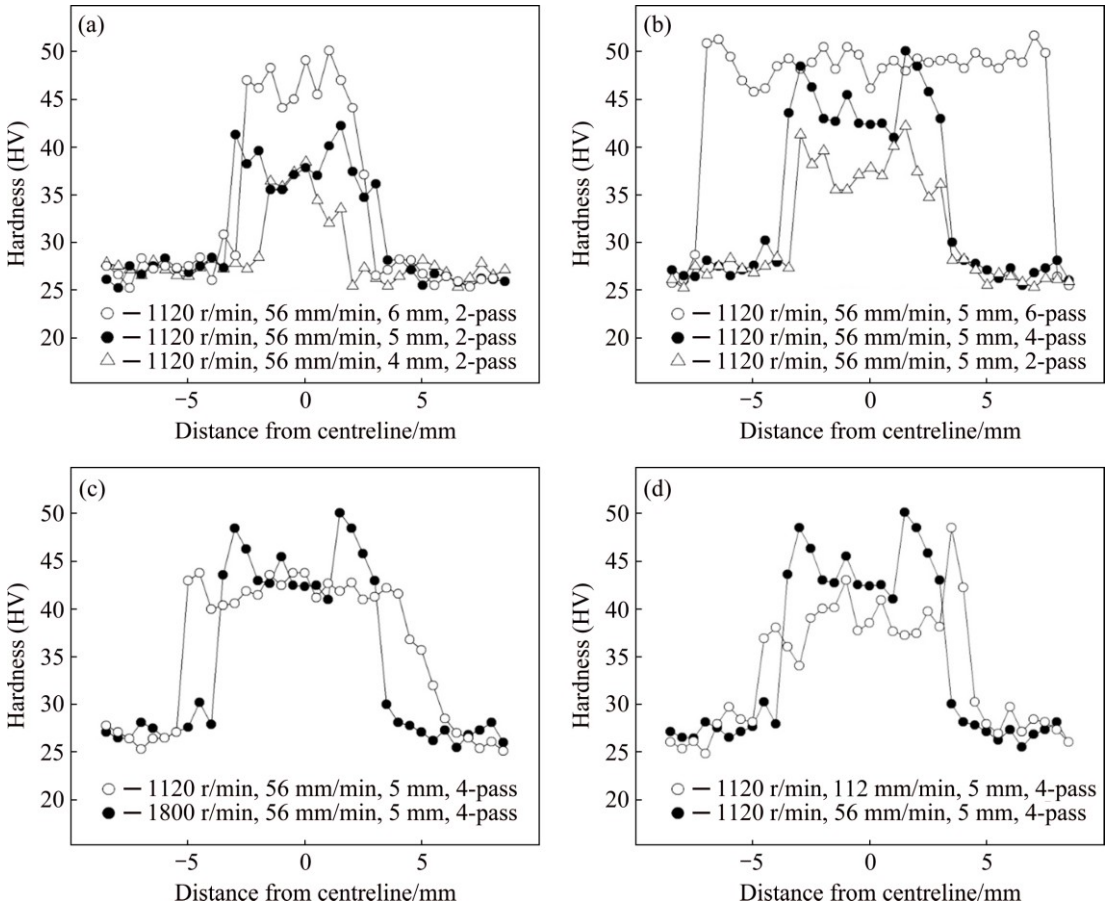

Fig. 5 Hardness profiles of FSPed samples for different processing conditions: (a) Different pin parameters; (b) Different FSP passes; (c) Different rotation speeds; (d) Different travel speeds

microhardness. High or low values of this ratio lead to low microhardness in comparison with the medium ratio case [31]. At the high ratio, due to higher heat input, grain growth results in lower microhardness according to the Hall−Petch relation. On the other hand, at the low ratio, poor distribution of particles leads to lower and heterogeneous microhardness values. It is worth to note that at high ratio, due to adequate particles distribution, a homogenous microhardness was obtained.

As demonstrated in Fig. 5, in general, the microhardness values within the stir zone were not symmetric and the uneven results were obtained. This is due to the banding structure which was mentioned in the previous reports [8].

The possible strengthening mechanisms which may operate in particle-reinforced metal matrix composites are [32]: 1) Orowan strengthening, 2) grain and substructure strengthening, 3) quench hardening due to the dislocations generated to accommodate the differential thermal contraction between the reinforcing particles and the matrix, and 4) work hardening, due to the strain misfit between the elastic reinforcing particles and the plastic matrix. According to the characteristics of the microstructure, the major contributions to the microhardness of the Al−Al_2Cu composites fabricated by FSP are: 1) the fine grain size of the Al matrix and 2) the Orowan strengthening due to the fine dispersion of Al_2Cu particles. The contribution of the fine grain size can be calculated from the Hall−Petch equation. The Hall−Petch relation for the hardness is $H_v=H_0+k_Hd^{-1/2}$, where H_0 and k_H are the constants. According to SATO et al [33], the values for the FSPed Al alloy are $H_0\approx$ 18 HV and $k_H\approx$19 HV·μm$^{1/2}$. For the FSPed samples, the microhardness values calculated from this equation are listed in Table 1. As can be seen in the table, there is a difference between the experimental and calculated values of microhardness, which is due to reinforcement strengthening. This value varies according to the FSP conditions (Fig. 6). As illustrated in Fig. 6, the highest reinforcement strengthening occurs in the samples FSPed using the pin of 6 mm diameter or the FSPed samples after the 6th pass. This is attributed to proper particle distributions in these samples.

Comparison of the present study with the previous ones indicates that the microhardness values reported in the previous works are higher than those of the current study [34−37]. This is may be due to the microvoids formation in the composite which reduce the microhardness.

3.4 XRD Results

Figure 7 shows the XRD results of the as-received and FSPed samples on the cross sections. The diffraction patterns show that Cu reacted with Al to form Al_2Cu, but some unreacted Cu remained even after the 6th FSP pass. The time that material is affected by the rotating pin in FSP can be considered as the processing time. Based upon the pin diameter and the tool traversing speed, the processing time is estimated to be ~8 s. That it, the formation of Al_2Cu phase is rapid in FSP. Previous study [20] suggested that severe plastic deformation during FSP would enhance the solid diffusion and decrease the reactive activation energy, thereby inducing the Al−Cu reaction to form Al_2Cu and particles in the matrix. The formation mechanisms of Al_2Cu were determined to be deformation-assisted solution-precipitation and interfacial reaction [23].

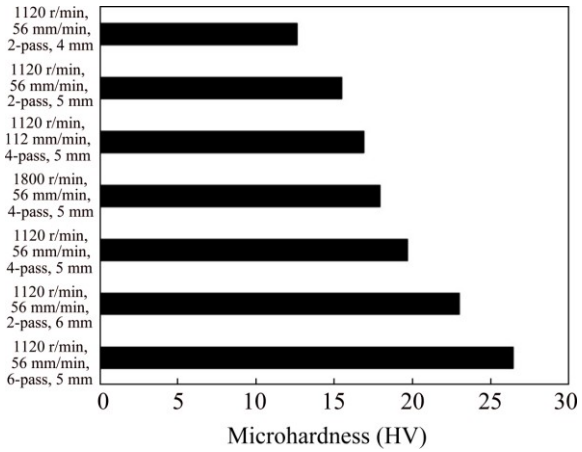

Fig. 6 Differences of experimental and calculated hardness values

As illustrated in Fig. 7, with the increase of heat input or the number of FSP passes, due to higher temperature and material flow, the formation of Al_2Cu is increased. However, there is no sign of Al_2Cu formation after only the 2nd pass of FSP even in the tool with 6 mm pin diameter. In addition, the peaks were shifted to higher 2θ values. These can be attributed to the associated process features (i.e., texture and strain). Furthermore, the Cu or Al_2Cu peaks are clearly broadened. Peak broadening indicates the introduction of higher dislocation density and smaller crystalline size of these particles.

In the as-received material, the measured (220) peak is much stronger than the calculated intensity assuming the random texture, which reveals the initial recrystallized rolling texture in the as-received Al plate. And the measured intensity of the (111) peak is slightly weaker than the random texture case. However, in the FSPed samples, the measured peak intensity of the (111) plane is higher than the calculated intensity. This implies that the (111) plane tends to lie on the transverse plane of the FSPed samples (or perpendicular to the pin travel direction) [38]. With an increase of heat input in the samples FSPed at 1800 r/min, the induced higher

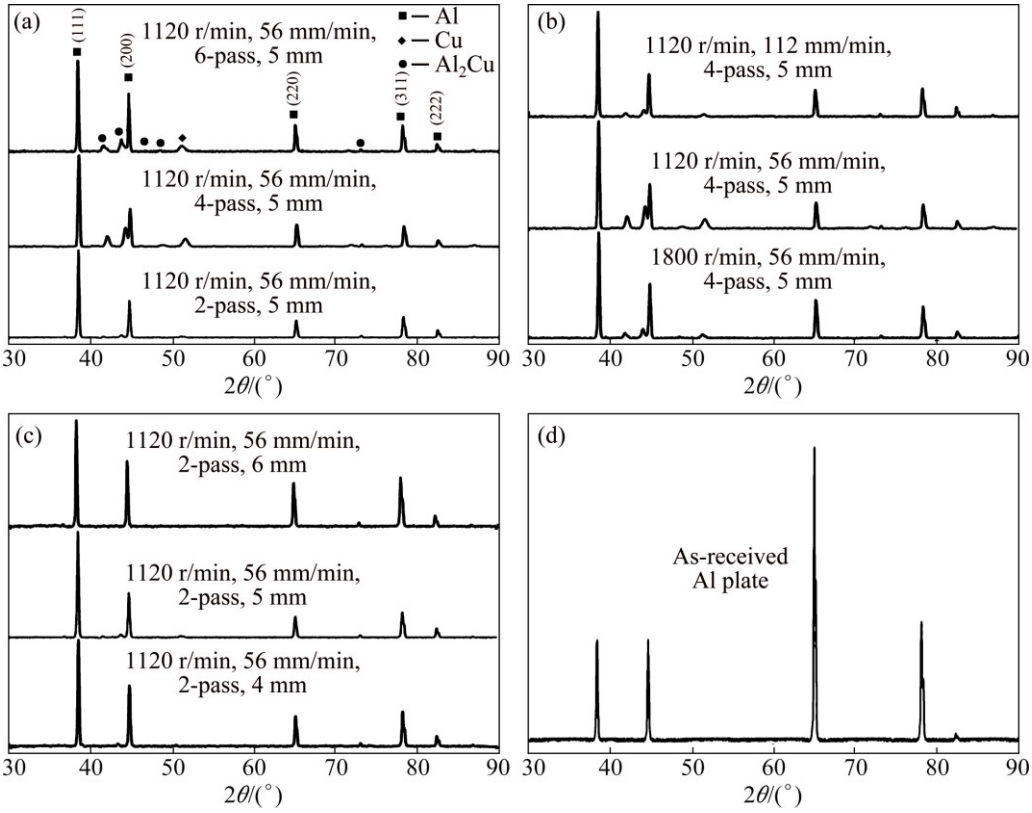

Fig. 7 XRD patterns of FSPed samples: (a) Different FSP passes; (b) Different rotation speeds; (c) Different pin parameters; (d) As-received Al plate

temperature rise result in more complete dynamic recrystallization (DRX), as well as more random orientation. Due to a similar reason, further FSP leads to more random orientation due to higher DRX.

4 Conclusions

1) The pin diameter has a higher effect on the particle distribution and microhardness than the number of FSP passes and rotation-to-travel speed ratio.

2) The large plastic strain and high temperature introduced in FSP lead to the rapid exothermic reaction between Al and Cu to form in situ Al_2Cu phase.

3) The rapid formation of the Al_2Cu phase can be attributed to the mechanically activated effect of FSP.

4) Microstructure was slightly refined during the FSP of AA1100 alloy due to the dynamic recrystallization mechanism. By introducing reinforcing particles and formation of in situ intermetallic, the grain size in the stir zone was refined considerably due to the role of nano-metric particles on operating PSN and Zener−pinning mechanisms during DRX.

5) Owing to the formation of intermetallic nanoparticles and dispersion through the Al matrix, the Vickers microhardness of the prepared in situ nanocomposite was increased by 57% in comparison with the base metal.

6) Even after the 6th pass of FSP, some microvoids as well as unreacted Cu nanoparticles were observed in the composite.

7) Irregular morphology of the interface between Cu and the Al matrix is attributed to the local melting and therefore rapid reaction of Cu with the base metal.

Acknowledgements

M. AZIZIEH, D. IRANPARAST, M. A. G. DEZFULI and Z. BALAK gratefully acknowledge Islamic Azad University, the Ahwaz Branches for financial support of this research work.

References

[1] SURYANARAYANA C. Synthesis of nanocomposites by mechanical alloying [J]. Journal of Alloys and Compounds, 2011, 509: 229−234.

[2] SURYANARAYANA C, AL−AQEELI N. Mechanically alloyed nanocomposites [J]. Progress in Materials Science, 2013, 58: 383−502.

[3] HEMANTH J. Development and property evaluation of aluminium alloy reinforced with nano-ZrO_2 metal matrix composites (NMMCs) [J]. Materials Science and Engineering A, 2009, 507:110−113.

[4] BOGUE R. Nanocomposites: A review of technology and applications [J]. Assembly Automation, 2011, 31: 106−112.

[5] PROVENZANO V, HOLTZ R L. Nanocomposites for high temperature applications [J]. Materials Science and Engineering A, 1995, 204: 125−134.

[6] SURYANARAYANA C. Mechanical alloying and milling [J]. Progress in Materials Science, 2001, 46: 1−184.

[7] CHEN W, LIU Y, YANG C, ZHU D, LI Y. (SiC_p+Ti)/7075Al hybrid composites with high strength and large plasticity fabricated by squeeze casting [J]. Materials Science and Engineering A, 2014, 609: 250−254.

[8] AZIZIEH M, KOKABI A H, ABACHI P. Effect of rotational speed and probe profile on microstructure and hardness of AZ31/Al_2O_3 nanocomposites fabricated by friction stir processing [J]. Materials and Design, 2011, 32: 2034−2041.

[9] NARIMANI M, LOTFI B, SADEGHIAN Z. Evaluation of the microstructure and wear behaviour of AA6063−B4C/TiB2 mono and hybrid composite layers produced by friction stir processing [J]. Surface and Coatings Technology, 2016, 285: 1−10.

[10] CHEN Z, LI J, BORBELY A, JI G, ZHONG S Y, WU Y, WANG M L, WANG H W. The effects of nanosized particles on microstructural evolution of an in−situ TiB_2/6063Al composite produced by friction stir processing [J]. Materials and Design, 2015, 88: 999−1007.

[11] GOLMOHAMMADI M, ATAPOUR M, ASHRAFI A. Fabrication and wear characterization of an A413/Ni surface metal matrix composite fabricated via friction stir processing [J]. Materials and Design, 2015, 85: 471−482.

[12] KHODABAKHSHI F, HAGHSHENAS M, SAHRAEINEJAD S, CHEN J, SHALCHI B, LI J, GERLICH A P. Microstructure property characterization of a friction stir welded joint between AA5059 aluminum alloy and high density polyethylene [J]. Materials Characterization, 2014, 98: 73−82.

[13] HE X, GU F, BALL A. A review of numerical analysis of friction stir welding [J]. Progress in Materials Science, 2014, 65: 1−66.

[14] MICHAEL RAJAN H B, DINAHARAN I, RAMABALAN S, AKINLABI E T. Influence of friction stir processing on microstructure and properties of AA7075/TiB_2 in situ composite [J]. Journal of Alloys and Compounds, 2016, 657: 250−260.

[15] YOU G L, HO N J, KAO P W. Aluminum based in situ nanocomposite produced from Al−Mg−CuO powder mixture by using friction stir processing [J]. Materials Letters, 2013, 100: 219−222.

[16] YOU G L, HO N J, KAO P W. The microstructure and mechanical properties of an Al−CuO in-situ composite produced using friction stir processing [J]. Materials Letters, 2013, 90: 26−29.

[17] QIAN J, LI J, XIONG J, ZHANG F, LIN X. In situ synthesizing Al_3Ni for fabrication of intermetallic−reinforced aluminum alloy composites by friction stir processing [J]. Materials Science and Engineering A, 2012, 550: 279−285.

[18] SHAHI A, HEYDARZADEH SOHI M, AHMADKHANIHA D, GHAMBARI M. In situ formation of Al−Al_3Ni composites on commercially pure aluminum by friction stir processing [J]. The International Journal of Advanced Manufacturing, 2014, 79(9−12): 1331−1337.

[19] SARKARI KHORRAMI M, SAMADI S, JANGHORBAN Z, MOVAHEDI M. In−situ aluminum matrix composite produced by friction stir processing using Fe particles [J]. Materials Science and Engineering A, 2015, 641: 380−390.

[20] DINAHARAN I, ASHOK KUMAR G, VIJAY S J, MURUGAN N. Development of Al_3Ti and Al_3Zr intermetallic particulate reinforced aluminum alloy AA6061 in situ composites using friction stir processing [J]. Materials and Design, 2014, 63: 213−222.

[21] ZHANG Q, XIAO B L, MA Z Y. In situ formation of various intermetallic particles in Al−Ti−X(Cu, Mg) systems during friction stir processing [J]. Intermetallics, 2013, 40: 36−44.

[22] YOU G L, HO N J, KAO P W. In-situ formation of Al_2O_3 nanoparticles during friction stir processing of Al single bond SiO_2 composite [J]. Materials Characterization, 2013, 80: 1−8.

[23] KRISHNAN K N. On the formation of onion rings in friction stir welds [J]. Materials Science and Engineering A, 2002, 327: 246−251.

[24] MISHRA R S, MA Z Y. Friction stir welding and processing [J]. Materials Science and Engineering R, 2005, 50: 1−78.

[25] BARMOUZ M, GIVI M K B, SEYFI J. On the role of processing parameters in producing Cu/SiC metal matrix composites via friction stir processing: Investigating microstructure, microhardness, wear and tensile behavior [J]. Materials Characterization, 2011, 62: 108−117.

[26] AMMOURI A H, KRIDLI G, AYOUB G, HAMADE R F. Relating grain size to the Zener−Hollomon parameter for twin-roll-cast AZ31B alloy refined by friction stir processing [J]. Journal of Materials Processing Technology, 2015, 222: 301−306.

[27] TANG W, GUO X, MCCLURE J C, MURR L E, NUNES A. Heat input and temperature distribution in friction stir welding [J]. Journal of Materials Processing & Manufacturing Science, 1998, 7: 163−172.

[28] DOHERTY R D, HUGHES D A, HUMPHREYS F J, JONAS J J, JUUL JENSEN D, KASSNER M E, KING W E, MCNELLEY T R, MCQUEEN H J, ROLLETT A D. Current issues in recrystallization: A review [J]. Materials Science and Engineering A, 1997, 238: 219−274.

[29] CHANG C I, LEE C J, HUANG J C. Relationship between grain size and Zener−Holloman parameter during friction stir processing in AZ31 Mg alloys [J]. Scripta Materialia, 2004, 51: 509−514.

[30] AHN B W, CHOI D H, KIMY H, JUNG S B. Fabrication of SiCp/AA5083 composite via friction stir welding [J]. Transactions of Nonferrous Metals Society of China, 2012, 22: s634−s638.

[31] FELIX XAVIER MUTHU M , JAYABALAN V. Effect of pin profile and process parameters on microstructure and mechanical properties of friction stir welded Al−Cu joints [J]. Transactions of Nonferrous Metals Society of China, 2016, 26: 984−993.

[32] LLOYD D J. Particle reinforced aluminium and magnesium matrix composites [J]. International Materials Reviews, 1994, 39: 1−23.

[33] SATO Y S, URATA M, KOKAWA H, IKEDA K. Hall−Petch relationship in friction stir welds of equal channel angular−pressed aluminium alloys [J]. Materials Science and Engineering A, 2003, 354: 298−305.

[34] SATHISKUMAR R, DINAHARAN I, MURUGAN N, VIJAY S J. Influence of tool rotational speed on microstructure and sliding wear behavior of Cu/B_4C surface composite synthesized by friction stir processing [J]. Transactions of Nonferrous Metals Society of China, 2014, 24: 95−102.

[35] DEVARAJU A, KUMAR A, KOTIVEERACHARI B. Influence of addition of Gr_p/Al2O3$_p$ with SiC_p on wear properties of aluminum alloy 6061-T6 hybrid composites via friction stir processing [J]. Transactions of Nonferrous Metals Society of China, 2013, 23: 1275−1280.

[36] CHOI D H, KIM Y H, AHN B W, KIM Y I, JUNG S B. Microstructure and mechanical property of A356 based composite by friction stir processing [J]. Transactions of Nonferrous Metals Society of China, 2013, 23: 335−340.

[37] CHOI D H, KIM Y I, KIM D U, JUNG S B. Effect of SiC particles on microstructure and mechanical property of friction stir processed AA6061-T4 [J]. Transactions of Nonferrous Metals Society of China, 2012, 22: s614−s618.

[38] GAN W Y, ZHOU Z, ZHANG H, PENG T. Evolution of microstructure and hardness of aluminum after friction stir processing [J]. Transactions of Nonferrous Metals Society of China, 2014, 24: 975−981.

采用摩擦搅拌工艺制备 Al/Al_2Cu 原位纳米复合材料

M. AZIZIEH[1], D. IRANPARAST[1], M. A. G. DEZFULI[1], Z. BALAK[1], H. S. KIM[2]

1. Department of Materials Science and Engineering, College of Engineering,
Ahvaz Branch, Islamic Azad University, Ahvaz 61349-37333, Iran;
2. Department of Materials Science and Engineering,
Pohang University of Science and Technology (POSTECH), Pohang 790−784, Korea

摘　要：采用摩擦搅拌工艺制备 Al/Al_2Cu 原位纳米复合材料，研究摩擦搅拌工艺参数如旋转速率、行进速率、搅拌道次和搅拌针形状对铝基纳米复合材料显微组织、化学反应和显微硬度的影响。由于摩擦搅拌工艺的机械活化效应以及 Al−Cu 放热反应产生大量的热，Al_2Cu 粒子快速形成。纳米复合材料的显微组织包含细小晶粒的铝基体(~15 μm)、未反应的铜纳米粒子以及 Al_2Cu 纳米强化相。Al_2Cu 粒子的不规则形貌是由于摩擦搅拌过程中产生局部熔化。搅拌针直径对材料的显微组织和硬度具有较大的影响。与基体合金相比，所得复合材料的硬度提高了 57%。

关键词：摩擦搅拌工艺；复合材料；硬度；显微组织；表面性能

(Edited by Yun-bin HE)